Taylor & Francis
Taylor & Francis Group

Phase Transitions
A Multinational Journal

ISSN: 0141-1594 (Print) 1029-0338 (Online) Journal homepage: http://www.tandfonline.com/loi/gpht20

The $NaNO_3$–KNO_3 phase diagram

R. Benages-Vilau, T. Calvet, M.A. Cuevas-Diarte & H.A.J. Oonk

To cite this article: R. Benages-Vilau, T. Calvet, M.A. Cuevas-Diarte & H.A.J. Oonk (2016) The $NaNO_3$–KNO_3 phase diagram, Phase Transitions, 89:1, 1-20, DOI: 10.1080/01411594.2015.1083567

To link to this article: http://dx.doi.org/10.1080/01411594.2015.1083567

Published online: 22 Oct 2015.

Submit your article to this journal

Article views: 35

View related articles

View Crossmark data

Full Terms & Conditions of access and use can be found at
http://www.tandfonline.com/action/journalInformation?journalCode=gpht20

Download by: [University Library Utrecht] **Date:** 27 January 2016, At: 06:48

Phase Transitions, 2016
Vol. 89, No. 1, 1–20, http://dx.doi.org/10.1080/01411594.2015.1083567

Taylor & Francis
Taylor & Francis Group

The $NaNO_3$–KNO_3 phase diagram

R. Benages-Vilau[a]*, T. Calvet[a], M.A. Cuevas-Diarte[a] and H.A.J. Oonk[b]

[a]*Departament de Cristal·lografia, Mineralogia i Dipòsits Minerals, Facultat de Geologia, Universitat de Barcelona (UB), Barcelona, Spain;* [b]*Department of Earth Sciences, Utrecht University, Utrecht, The Netherlands*

(*Received 4 March 2015; accepted 6 August 2015*)

Many papers have been published in relation to the $NaNO_3$–KNO_3 phase diagram determination in the last 160 years. These papers fall in two categories: (1) the solid–liquid equilibrium is assumed to be of the eutectic type, and (2) the solid–liquid equilibrium is considered as a loop with a minimum. The discordance between the two views is related to the slow transition kinetics that complicate the assessment of thermal 'fluctuations', and also to the appearance of a metastable form of potassium nitrate. The main result of this paper is the experimental phase diagram constructed with new experimental data so that we can assure that the second option is correct. This phase diagram is defined by a eutectoid invariant, an asymmetric immiscibility gap and a continuous solid solution with a minimum of melting point. Additionally, the *AB*θ model simulates correctly the experimental piece of evidence.

Keywords: solid solution; miscibility; XRD; phase diagram

Downloaded by [University Library Utrecht] at 06:48 27 January 2016

Introduction

The first $NaNO_3$–KNO_3 paper known was published in 1857.[1] Since then, many publications have appeared including a handbook.[2] A quick look at them permits us to make the following classification: (1) papers in which the solid–liquid equilibrium is held for eutectic (limited subsolidus miscibility); and (2) papers in which it is represented by a loop with a minimum (evidence of complete subsolidus miscibility; continuous solid solution). In the older papers reviewed a eutectic system is proposed, followed by a continuous solid solution in the most recent literature,[1] while in the most recent publications, the notion of eutectic behaviour becomes prevalent again.[1,3–5] Thus, for more than 160 years, the following question has remained unanswered: Is the phase diagram described by eutectic behaviour or a melting point minimum? Phase diagram determination poses significant experimental difficulties as will be described in this paper and the solid-state region has been studied only partially – a complete thermodynamic explanation for the whole diagram is still to be published – which explains the lack of conclusive evidence on the topic.

To describe a phase diagram, first we need to know the polymorphism of its components. An extensive summary of alkali nitrates polymorphism has been provided by Rao et al.[6] in 1975 and updated by Benages-Vilau et al. in a recent paper.[7] The main polymorphic characteristics of $NaNO_3$ and KNO_3 are described briefly in next paragraphs and schematically shown in Figure 1. The crystallographic parameter values are shown in Table 1.

*Corresponding author. Email: rbenages@irec.cat

© 2015 Taylor & Francis

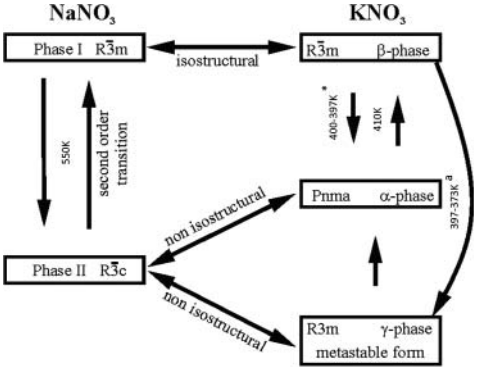

Figure 1. $NaNO_3$ and KNO_3 polymorphic and isostructural relationships. *β-KNO_3 to α-KNO_3 transition is reversible only for a temperature range of 400−397 K.[a]The β-KNO_3 to γ-KNO_3 transition temperature depends on many factors. See Ref. [7] for more information.
Notes: '*' makes reference to R-3m to Pnma transition of potassium nitrate.
'a' makes reference to R-3m to R3m transition of potassium nitrate.

Of relevant importance for this system are the phase transitions of the components.

(1) $NaNO_3$ shows a λ transition and it is discussed as a second-order phase transition (order−disorder) range of some 100 K.[9,10] In fact, it has been regarded as a particularly suitable system for testing certain theories and relations proposed for higher order transitions.[11] As far as we know, there are few reports in the literature that have considered these implications using differential scanning calorimetry (DSC) or other techniques. For example, Klement [12] was able to follow the transition until 10% of KNO_3 with DSC, while Ping et al. [5] were able to follow it until 50% of KNO_3. However, they assigned two transitions for the equimolar composition, which has no thermodynamic significance. X-ray diffraction (XRD), which is the best technique to examine this gradual transition, was performed for $NaNO_3$ and/or $CaCO_3$ (isostructural compounds) by Antao and coworkers,[13,14] Ballirano [15] and Harris.[16]

Therefore, high temperature XRD (HTXRD) is mandatory to elucidate how this transition affects this phase diagram. We point out that some authors have missed its influence.[17,18]

(2) For KNO_3, the metastable γ-KNO_3 introduces some difficulties in the system. γ-KNO_3 is observed when crystals are cooled from temperatures above 453 K, but it does not appear when crystals are heated from the α-form.[19] Nimmo and Lucas [20] found that the γ-KNO_3 phase could be cooled to room temperature

Table 1. Selected cell parameters for $NaNO_3$ and KNO_3 phases.

Phase	a/Å	b/Å	c/Å	Ref.
I − $NaNO_3$−R$\bar{3}$c	5.070		16.82	[8]
II − $NaNO_3$−R$\bar{3}$m	5.0889(5)		8.868(3)	[9]
α-KNO_3 Pnma	6.4213	5.4119	9.1567	[7]*
β−KNO_3R$\bar{3}$m	5.425(1)		9.836(4)	[19]
γ-KNO_3 R3m	5.487(1)		9.156(3)	[19]

Note: *after transforming the Pmcn space group to the international accepted by IUCr.

Downloaded by [University Library Utrecht] at 06:48 27 January 2016

and remain stable for approximately 30 minutes. Furthermore, the stability of the γ-KNO_3 phase depends on the manner of preparation, particle size, thermal history, impurities in the sample [21] and cooling rate.[22] Additionally, the hydrostatic stress may be responsible for the extended γ-KNO_3 phase stability in small particles.[23] Some attempts to stabilize the γ-phase at room temperature have been reported in the literature.[21,24–28] To close, Fermor and Kjekshus [29] highlight that when KNO_3 is heated at 468 K, it recrystallizes, a necessary step for the γ-$KNO_3 \rightarrow \beta$-KNO_3 transition on cooling.

The structural similarities of the different forms can be discussed paying attention to the possibility of forming solid solutions. First, let us remember the basic rules: two substances that form a continuous series of mixed crystals (solid solutions) have equal structure characteristics, and commensurable molar volumes. The notion of 'equal structure characteristics' comes down to equal space group and the same arrangement of the structural units. The notion of 'commensurable molar volumes' can be best illustrated with the help of a practical example of the alkali halides that have the NaCl type of structure. The two substances, NaCl and KCl, for which the molar volume of the former is 28% less than the one of the latter, are miscible in all proportions above 500 °C. The two substances, KI and RbI, with a difference in molar volume of 11%, mix in all proportions already at room temperature.[30]

Within the six possible combinations for the structure of the $NaNO_3$–KNO_3 system, there is only one that fits the first requirement of having the same space group; β-KNO_3 and I-$NaNO_3$ have the same $R\bar{3}m$ space group and the same stacking sequence ABABAB… From the unit cell dimensions, ignoring any thermal expansion, it follows that the difference in molar volume is about 21%.

Another possibility is to find a γ-KNO_3-based solid solution because this phase is no substantially different from β-KNO_3.[20,31] Consequently, one might expect a narrow degree of miscibility between I-$NaNO_3$ and γ-KNO_3. Furthermore, the introduction of sodium in the γ-KNO_3 structure can, in certain ways, stabilize this hypothetical γ-KNO_3 solid solution type. Some examples are found in the literature.[21,28,32]

For the determination of this phase diagram, the most used technique is thermal analysis (cooling and heating curves before the advent of the methods of differential microcalorimetry, such as DSC and differential thermal analysis (DTA)).[4,7,33–39] Some authors used the data from the second heating run [4,33,35,36] (generally these data are in line with a third heating run, which is seen as evidence for the system having arrived at equilibrium). This fact can introduce errors in the determination of the equilibrium phase diagram. In some of the early investigations, chemical analyses were carried out of coexisting solid and liquid phases, in order to determine the positions of solidus and liquidus. [40–43] Kofler,[44] who used a heating microscope, stated that it was very difficult to differentiate between the two components.

Regarding thermal analysis, it should be mentioned that the nitrates are highly corrosive salts – as shown in Ellingham diagrams [45] – therefore, the selection of the appropriate DSC capsule is an important topic. Decomposition products (mainly NO_2) can react with aluminium, gold and platinum, particularly at high temperatures or during periods of prolonged exposure.[36,46–51]

Only four researchers have studied the mixed solid state by means of XRD. Kramer and Wilson [34] found rhombohedral $NaNO_3$ and orthorhombic KNO_3 patterns, when quenching both from above and below the liquidus line. They suggested that high temperature XRD is necessary to observe the solid solution. One year later, Kamimoto [35]

Downloaded by [University Library Utrecht] at 06:48 27 January 2016

worked with the equimolar composition using XRD at 473 K. He found a different XRD pattern and, in his opinion, a solid solution was formed. Unfortunately, he only gave stick patterns, which are difficult to interpret. He also observed the presence of γ-KNO_3 upon cooling and although he did not recognize it as such, he pointed out that the sample was not in a thermodynamically stable state. Abe et al. [37] only observed immiscibility at room temperature. Zhang et al. [39] measured, by XRD, an equimolar mixture at 473 K and found a superposition of β-KNO_3 and I-$NaNO_3$ patterns. Additionally, Xu and Chen [32] argued that XRD would give a structure with a level of symmetry higher than that measured by spectroscopic techniques in disordered systems.

In some papers, a calculated phase diagram is shown; it is either eutectic [4,39] or shows a solid−liquid loop with a minimum.[18,38] In 1990, Dessureault et al. [18] published a review of more than 30 papers. They conducted a statistical analysis of the thermodynamic data presented in these papers. They constructed a thermodynamic model for the system, and calculated a solid−liquid loop with a minimum. A very recent paper suggests the contrary,[52] they propose a eutectic-type phase diagram. However, careful reading of this paper indicates that the eutectic shape is imposed by the authors after reading the papers from Xu and Chen [32,52] and Berg and Kerridge.[3]

Another technique widely used in recent years is the Raman spectroscopy and all researchers who used it concluded that the $NaNO_3$−KNO_3 phase diagram shows eutectic behaviour.[1,3,32,53] Mechanical characterization [54] and electrical measurements throughout the melting process [55,56] were also tried to address the problem.

Special attention must be given to the classical work by Tammann and Ruppelt published in 1931.[40] The two investigators applied the technique of cooling and heating curves, and completed their experiments with microscopic observations. They made two significant observations. First, crystals that had crystallized from the equimolar mixture had grown when kept at a 200 °C. According to the investigators, it is an evidence of the formation of a solid solution; a eutectic conglomerate would not do so. Second, the clear crystals that had crystallized from the melt became turbid on cooling at a given temperature as a function of composition. The onset temperature of turbidity was taken as the temperature at which the homogeneous sample enters the two-phase region. The minimum of the solid−liquid loop is about at 494 K and at the equimolar composition. The critical point of (solid-state) mixing, the top of the miscibility gap, is at about 448 K and between 40% and 50% KNO_3.

Our group has extensive experience in polymorphism [30,57−60] and the phase diagram determination,[61,62] and our publications show the importance of using complementary techniques to effectively establish the stability regions within a binary system. From this position, we decided to study the $NaNO_3$−KNO_3 system, in order to arrive at a conclusive answer to the true nature of the solid−liquid and solid−solid equilibrium. It is worth saying that in this paper XRD is the selected technique to characterize the equilibrium state of different phase domains. Other complementary techniques, DSC, Raman and hot stage microscopy are used to check results obtained by XRD.

Materials and methods

High purity $NaNO_3$ and KNO_3 (99% or higher) were supplied by Quality Chemicals.[63] The purity of these nitrates was checked with inductively coupled plasma optical emission spectrometry (ICP-OES), revealing the impurities (in the ppm range) in $NaNO_3$ and KNO_3, to be K^+ and Na^+, respectively. Further purification was therefore not carried out. Water content in pure compounds was checked by thermogravimetry (being less than 0.3%).

Downloaded by [University Library Utrecht] at 06:48 27 January 2016

Downloaded by [University Library Utrecht] at 06:48 27 January 2016

Samples of 1 g of selected binary compositions (in total, there were 17 different samples, including pure compounds) were weighed in the correct molar proportions with an accuracy of 1 mg. They were melted and quenched inside a Pyrex glass tube in liquid nitrogen, then grounded and stored at room temperature.

Thermal analyses were performed with a Perkin Elmer DSC-7. We carried out many experiments to determine the most effective configuration. In this paper, we use aluminium capsules with holes, a sample weight of between 4.4 and 4.8 mg, a heating rate of 10 K/min and the upper temperature was approximately 10 K higher than the liquidus line for each composition. Working in this way, we have not noticed reaction between samples and aluminium capsules. Except for some samples, only two independent runs were carried out for each one of them. The DSC-7 was calibrated against indium and n-decane standards. From the DSC curve we have determined the onset temperature by extrapolation of the slopes and the ending temperature of the process by applying the shape factor, the enthalpy effects were evaluated integrating the DSC signals.[64] X-ray powder diffraction data was recorded with a Panalytical X'pert Pro diffractometer at room temperature with the Bragg−Brentano geometry ($\theta - 2\theta$). The pattern was acquired over a period of 39 minutes within a range of 4° to 100° (2θ) using Cu $K_{\alpha 1}$ radiation ($\lambda =$ 1.5405 Å). Samples were mounted on a flat automatic sample charger. A spin rotation of 2 rev/min was selected to minimize the preferred orientation of the sample. The diffractometer was equipped with a hybrid monochromator and an X'Celerator detector. Temperature-dependent XRD was recorded with the same geometry for all compositions using an Anton Paar HTK-1200 N oven. Acquisition temperatures were set at 301−323−373−393−403−413−473−493−523−553−563−573−583−593 K for a period of 2 h at each temperature. Stabilization time at each temperature was 5 minutes except at 393 K, which was 15 minutes to try achieving equilibrium. Additionally, a heating rate of 10 K/min was used and a maximum temperature depending on the sample melting point.

For selected compositions, in order to achieve equilibrium at high temperatures, annealing at various temperatures was carried out for up to 7 days in a FURCAP device from INEL diffractometer, which enables capillary samples to be heated from room temperature to 623 K. An X-ray powder diffraction pattern was collected after every 2 h of exposure. The sample is continuously rotated to minimize a preferred orientation. In this case, the diffraction patterns were recorded in a horizontally mounted 120° and 25 cm of radius curved position sensitive detector INEL CPS-120 in transmission geometry. The detector was used in its 4096 channels resolution mode. Samples were placed in 0.5 mm diameter glass Lindemann capillaries. Cu $K\alpha_1$ radiation was selected by means of a Ge (111) primary flat monochromator. A parabolic multiplayer mirror 'OSMIC Gutman optics # 13B-413' was placed between the tube and the monochromator. $Na_2Ca_3Al_2F_{14}$ was used as an external standard to calibrate the detector and convert the channels to 2θ values. The data were linearized to a constant step size of 0.029° in 2θ by means of a cubic spline function. Calibration and linearization were performed with the PEAKOC application from DIFFRACTINEL software.

Materials Studio software was used for the cell parameter determination in some powder patterns,[65] while peak intensity and peak wideness were determined using the WinplotR software. Taking at least eight reflections of apparently well-separated peaks, the X-CELL indexing program [66] found the potential solutions of cell parameters and space groups. Those that best corresponded to the experimental XRD pattern were finally obtained using a Pawley profile-fitting procedure [67] available in the Powder Indexing module of Materials Studio.

A Raman spectroscopy study was carried out at room temperature with a Jobin Yvon T64000 Raman spectrometer. A liquid nitrogen cooled CCD detector was calibrated against TiO_2 and nominal laser power was 400 mW with a 514 nm wavelength. Five measurements of 10 sec each were performed from 24 to 1700 cm^{-1}. Peak position and peak intensity were measured with the Origin Software.

For hot stage microscopic measurements, a Linkam THMSG-600 stage mounted to a Nikon Eclipse 50iPol Microscope was used. The sample was placed on a 7 mm quartz cover slip, and encased within a pure silver lid so that it was heated from all sides, ensuring a uniform temperature. An LNP liquid nitrogen cooling system and a TMS94 temperature controller were used. Images were captured with a digital camera. In order to visualize the phase transition and the solidus line (on heating runs), a thin film was required. To obtain this, the sample was placed on a glass cover slip, heated above its melting point and then covered with another glass cover slip to obtain the thin film. The system was left for approximately 1 minute in the liquid state and was then finally cooled to room temperature at 100 K/min.

Experimental results

In this section, in a step-by-step manner, the results are presented of the experiments we carried out.

DSC and hot stage microscopy experiments

Generally, experiments by DSC provide information on the heat effect and the temperature characteristics of phase transitions. In our case, the experiments give information on (1) the eutectoid peak that goes together with the change of α-KNO_3 to β-KNO_3; and (2) the change from solid to liquid.

The DSC measurements were reproducible in temperature and enthalpy values. Representative results obtained for the first heating run as a function of composition are gathered in Table 2. Thermal analysis normally is very valuable to detect the change between

Table 2. Results for temperatures and enthalpies of phase transitions for the $NaNO_3-KNO_3$ system.

	Solid−solid transition					Solid−liquid transition			
(% mol KNO_3)	$T_{\alpha\rightarrow\beta}$ (K)	$T_{\text{end (II}\rightarrow\text{I)}}$ (K)	$T_{\text{eutectoid}}$ (K)	$T_{(\text{end eutectoid})}$ (K)	ΔH_{s-s} (J.mol^{-1})	T_{melting} (K)	T_{solidus} (K)	T_{liquidus} (K)	ΔH_{s-l} (J.mol^{-1})
0		544				581			15,435
10			394	398	410		494	567	13,433
20			395	397	930		494	545	12,561
30			394	395	1699		495	535	10,926
40			392	402	2180		494	503	10,223
50			396	399	2616		492	492	10,009
60			390	398	3192		495	505	9473
70			389	398	3743		495	530	9954
80			390	400	4105		494	554	9233
90			391	399	4634		495	586	10,308
100	404				5164	610			9498

Downloaded by [University Library Utrecht] at 06:48 27 January 2016

Downloaded by [University Library Utrecht] at 06:48 27 January 2016

phase domains. Due to the characteristics of the phase diagram in this paper, it does not give accurate descriptions of these changes in the entire phase diagram. Furthermore, our measurements are pretty similar (in shape) to those of Ping et al.[5]

In order to detail the eutectoid change, compositions (with a 10% gap) were cycled two times. In the first heating run, we observed the eutectoid peak for all compositions at approximately 393 K. For the second heating run, the solid−solid transition was only observed in certain compositions; this may have some relation to the influence of the γ-KNO_3 phase. To ascertain whether this was the case, some samples were recycled with a time lag (between either weeks or months) to test the solid−solid transition evolution. As expected, significant differences were observed. Baryshnikov demonstrated that while in the first run, II-$NaNO_3$ and β-KNO_3 coexist, in the second heating run, only the γ-KNO_3 type solid solutions seem to be present,[28] consistent with the results of our DSC stability experiments. As a result, we have to point out that all the experimental information available conducts us to propose that the first heating run starts from a stable state. The numerical values of the heat effects at the eutectoid temperature, as beautifully follows from the data in Table 2, are linear in composition − in agreement with the lever rule.[68]

Furthermore, a transition, probably a λ transition or even a second order, is detected only for high sodium nitrate content. This transition and the melting signal overlapped one another for some compositions because the continuous variation of the slope, characteristic from this transition, is supposed to be overlapped by the strong heat interchange of the melting signal.

In hot stage microscopy, only first-order solid−solid transitions could be studied, i.e. those related to KNO_3. The $\alpha-\beta$ transition on heating and the $\beta-\gamma$ transition on cooling were not destructive. In contrast, the $\gamma-\alpha$ transition is totally destructive causing crystals or domains to break into smaller pieces. Furthermore, since γ-phase is metastable at room temperature, the transition time changes in different experiments and different compositions, as was described in the Introduction section. When the temperature is above the eutectoid temperature, all the crystal phase boundaries move fast and tend to grow to achieve the minimum free energy in accordance with the Tamman and Ruppelt work.[40]

X-ray diffraction analyses at room temperature

XRD analyses were carried out at room temperature to assess the crystal phases. Diffractograms were indexed as the combination α-KNO_3 and II-$NaNO_3$, except for the extreme compositions (1% KNO_3 and 99% KNO_3) in which only the pure components are observed.

For the extreme compositions, XRD revealed somewhat wider- and less defined peaks. Minor component peak intensities for these compositions, if any, may be very close to the detection limit of XRD so they cannot be resolved from background.

For compositions from 1% KNO_3 to 20% KNO_3, a weak reflection at 27.10° of 2θ was visible, which can be assigned to the γ-KNO_3 phase. According to Westhphal,[23,24] the change γ-$KNO_3 \rightarrow \alpha$-KNO_3 can be considered as a cooperative phase transition. This explains that when the mass fraction is small, the transition is slower because each γ-KNO_3 particle has to nucleate its own path for phase transition. Therefore, part of the γ-KNO_3 phase can be retained as the result of a kinetic effect.

Raman spectroscopy analyses at room temperature

The narrow miscibility range at room temperature was confirmed by macro Raman measurements of 19 samples, including pure compounds. Figure 2 shows the most important

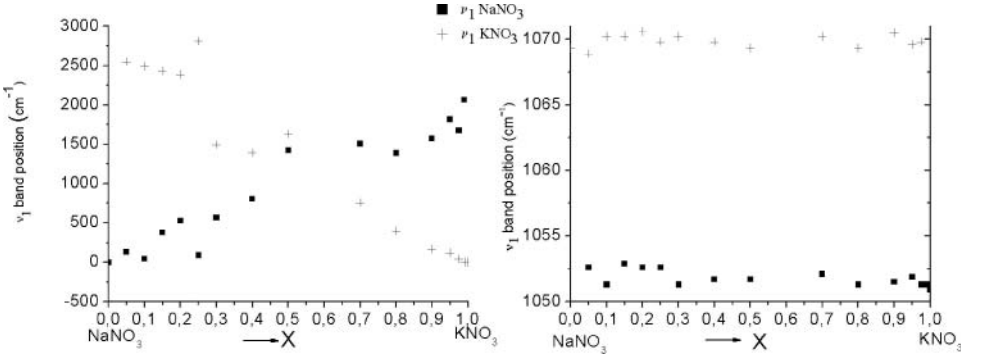

Figure 2. N−O stretching (ν_1) Raman band intensities (left) and position (right) for $NaNO_3$ (squares) and KNO_3 (crosses).

band positions and intensities, corresponding to the N−O stretching mode ν_1 at 1068 cm^{-1} and at 1049 cm^{-1} for $NaNO_3$ and KNO_3, respectively.[69] Intensity values are almost linear with composition, and the position of bands does not change within the experimental error. If sodium and potassium nitrate are miscible at room temperature, their miscibility range should be lower than 1%, which is in agreement with the results of Hissink [41] who stated that miscibility at room temperature was about 0.5%.

X-ray diffraction analysis as a function of temperature

As mentioned above, although this binary system has been studied for a long time, very few researchers have characterized mixed samples by XRD.

In Figure 3, the results are shown of our XRD experiments on samples having the equilimolar composition studied from 301 K to melting temperature. Here, we observe that from room temperature to 373 K, α-KNO_3 and II-$NaNO_3$ phases coexist. At 393 K, a phase change takes place, confirming the existence of a eutectoid invariant in accordance with the DSC data. Following this, between 393 and 473 K, peaks appear that can be assigned to a β-KNO_3 solid solution, but they are not well developed (some of them are marked with an arrow). Practically all the system is out of equilibrium above the eutectoid invariant when we analyse each composition at 10 K/min. As explained above, the different phase regions are assigned with XRD where annealing is performed to arrive at the equilibrium. The transition temperatures observed by DSC and evaluated by XRD coincide. Finally, and of vital importance, is to mention the appearance of a completely developed unique phase at 483 K − a result that is consistent with the findings of Kamimoto. [35] In fact, II-$NaNO_3$ diffraction peaks disappeared at 473 K, but transition was not complete because few peaks persist. If we compare diffraction at 473 and 483 K, we observe that only some peaks (encircled in Figure 4) persist while others disappear.

To proceed further, annealing experiments were carried out for selected compositions, at different temperatures and annealing times in order to reach the equilibrium state.

Figure 4 shows the integral breath for (101) X-ray reflection of the β-solid solution type and (104) for I-$NaNO_3$ solid solution type as a function of annealing time for 20 KNO_3 at 483 K. These results demonstrate the importance of annealing time in achieving the equilibrium. It can be seen that the integral width for both reflections decreases and then reaches an almost constant value after approximately 50 hours of annealing. The same findings were observed for the peaks intensity. The solvus line (transition from two

Downloaded by [University Library Utrecht] at 06:48 27 January 2016

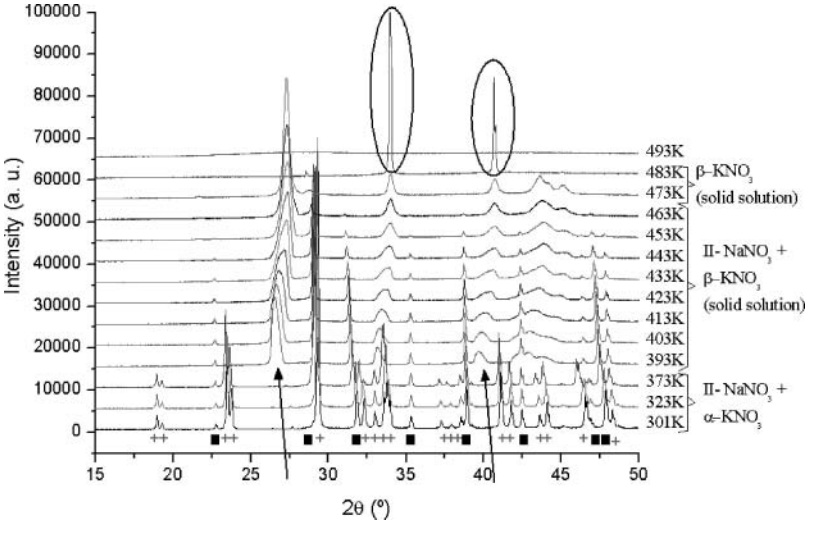

Figure 3. Powder X-ray diffraction as a function of temperature for the equimolar composition. Between temperatures of 301 and 373 K, II-$NaNO_3$ (squares) and α-KNO_3 (crosses) coexist. At 393 K, new peaks appear: arrows point to the α-$KNO_3 \rightarrow \beta$-KNO_3 transition. Encircled peaks indicate the phase, which appears at 483 K.

phases to one phase domain) cannot be measured by DSC because the transition is too slow and possibly the interchanged heat is small. Only the XRD at different temperatures permit us to determine this transition.

Samples of different compositions were kept for 48 hours at the four selected temperatures above the eutectoid invariant: 403, 433, 453 and 483 K, and then studied by the

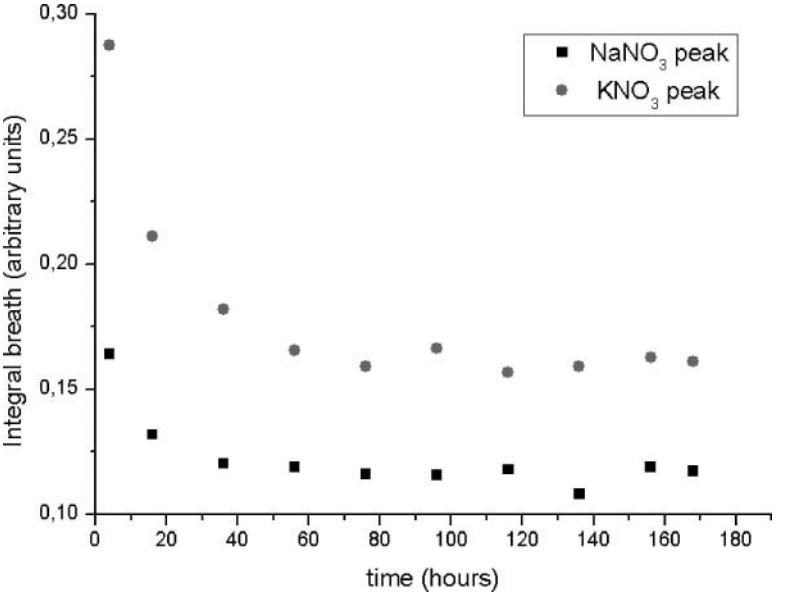

Figure 4. Integral width of diffraction peaks as a function of annealing time for 20 KNO_3 at 483 K. Figure shows II-$NaNO_3$ (squares) and β-KNO_3 (circles).

Downloaded by [University Library Utrecht] at 06:48 27 January 2016

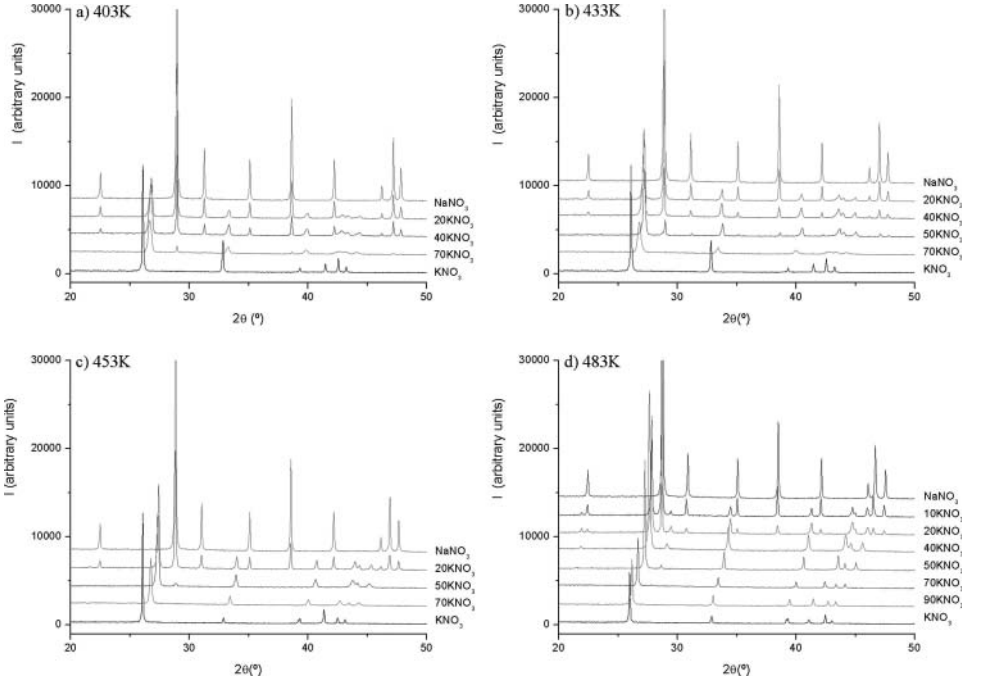

Figure 5. X-ray powder patterns as a function of the composition after 48 h of annealing at: (a) 403 K; (b) 433 K; (c) 453 K and (d) 483 K.

X-ray powder diffraction. For each temperature, the diffraction patterns are shown in Figure 5.

Figure 5(a), for 403 K, shows that the state of equilibrium is not yet achieved after 48 h. For the compositions 20% and 40% KNO_3, a single β-KNO_3 pattern type is observed together with (some peaks of) the II-$NaNO_3$ pattern. The β-KNO_3 reflections were displaced to 2θ higher values compared to pure KNO_3, indicating a smaller cell size, as a result of the introduction of sodium cations in the structure. Thus, a new phase appeared (as stated above), which was named β-solid solution because it has the same space group as β-KNO_3, $R\bar{3}m$. In contrast, the II-$NaNO_3$ pattern hardly changed, meaning that a significant amount of potassium did not enter the $R\bar{3}c$ structure of $NaNO_3$.

Figure 5(b), for 433 K, shows that for the 70% KNO_3 composition, only the β-solid solution is present, although it is not completely stable because the diffraction peaks are still relatively wide. For the remaining compositions analysed, the coexistence of β-solid solution and II-$NaNO_3$ patterns is observed, with a constant angle of 2θ, typical of an immiscibility zone.

In Figure 5(c), for 453 K, we notice that for the equimolar composition, the II-$NaNO_3$ type reflections have almost disappeared; only a minor II-$NaNO_3$ (104) reflection remains. This indicates an increasing presence of the β-solid solution, incorporating more sodium in its structure. For the 20% KNO_3 diffraction pattern, reflections due to II-$NaNO_3$ were slightly displaced to lower 2θ angle values (i.e. a larger unit cell) indicating that an amount of potassium is incorporated into its structure. Furthermore, a weak reflection at 21.6° is present, which can be indexed as (101) for the coexisting $R\bar{3}m$ phase (β-KNO_3 solid solution).

In Figure 5(d), for 483 K, the samples having compositions of 40% KNO_3 and higher are found to be homogeneous (β-solid solution space group $R\bar{3}m$). For lower potassium

Downloaded by [University Library Utrecht] at 06:48 27 January 2016

concentrations, a mixture between the β-solid solution and the II-$NaNO_3$ solid solution is observed. The diffraction lines of the $R\bar{3}c$ (II-$NaNO_3$) phase are displaced to lower 2θ angles compared to pure $NaNO_3$, indicating a higher unit cell compatible with the introduction of potassium in its structure, as explained above. Although the II-$NaNO_3$ solid solution single-phase domain must exist, we were unable to isolate it even by performing similar ageing experiments for the 5% KNO_3 composition.

From the previous analysis, we can deduce the space group and cell parameters, using the Materials Studio software.[64] Figure 6 shows the cell parameters (a and c) for these compositions together with pure KNO_3 and pure $NaNO_3$. As shown, Vegard's law is obeyed until 40% KNO_3, i.e. in all single-phase regions. For 40% KNO_3, 50% KNO_3, 70% KNO_3 and 90% KNO_3, a solution with the $R\bar{3}m$ symmetry was obtained. In all cases, the agreement between the experimental and simulated pattern expressed by the weighted R-factor (Rwp) was below 7%.

If we extrapolate the lines, we observe that they cut at approximately a and c/2 parameter for $NaNO_3$ composition; c parameter in $NaNO_3$ is halved in order to compare the same space group in both structures.[7]

When annealing is performed at 493 K, for 20% KNO_3 composition, the peaks of the II-$NaNO_3$ solid solution tend to disappear (results not shown). Nevertheless, 48 h was not enough time for completing the transition. We conclude that a single phase is also present in this composition but at higher temperatures.

All these results lead us to the main result of the paper: the experimental phase diagram shown in Figure 7. We assume that below the eutectoid, the solubility of Na^+ in α-KNO_3 is slightly higher than K^+ in the II-$NaNO_3$ structure, when kept at the same temperature. This is consistent with the fact that it is easier to introduce a smaller cation into a structure of larger cations than in the opposite case. Both the β-KNO_3 solid solution type and the II-$NaNO_3$ solid solution type have a narrow domain of existence with a maximum solubility at 393 (eutectoid invariant) and 483 K, respectively. Above the eutectoid

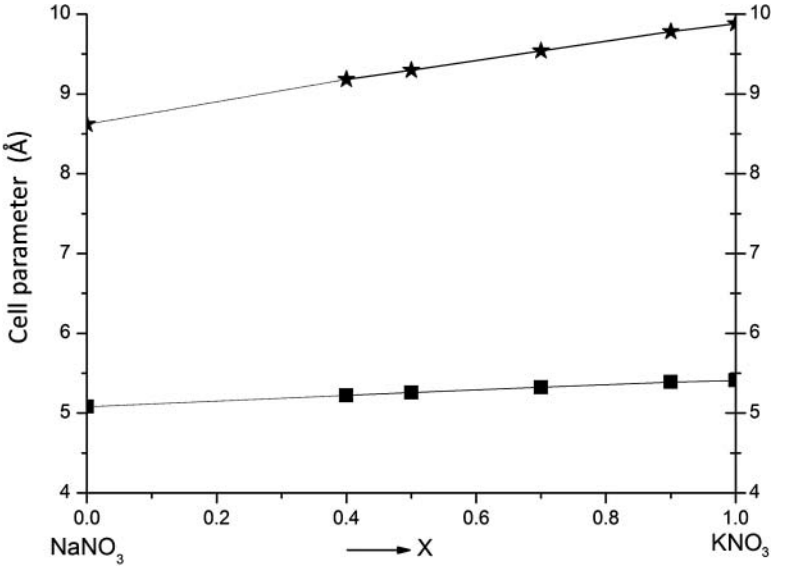

Figure 6. The evolution of cell parameters as a function of composition at 483 K. a cell parameter: square marks; c cell parameter:stars. (c parameter in $NaNO_3$ is halved).

Downloaded by [University Library Utrecht] at 06:48 27 January 2016

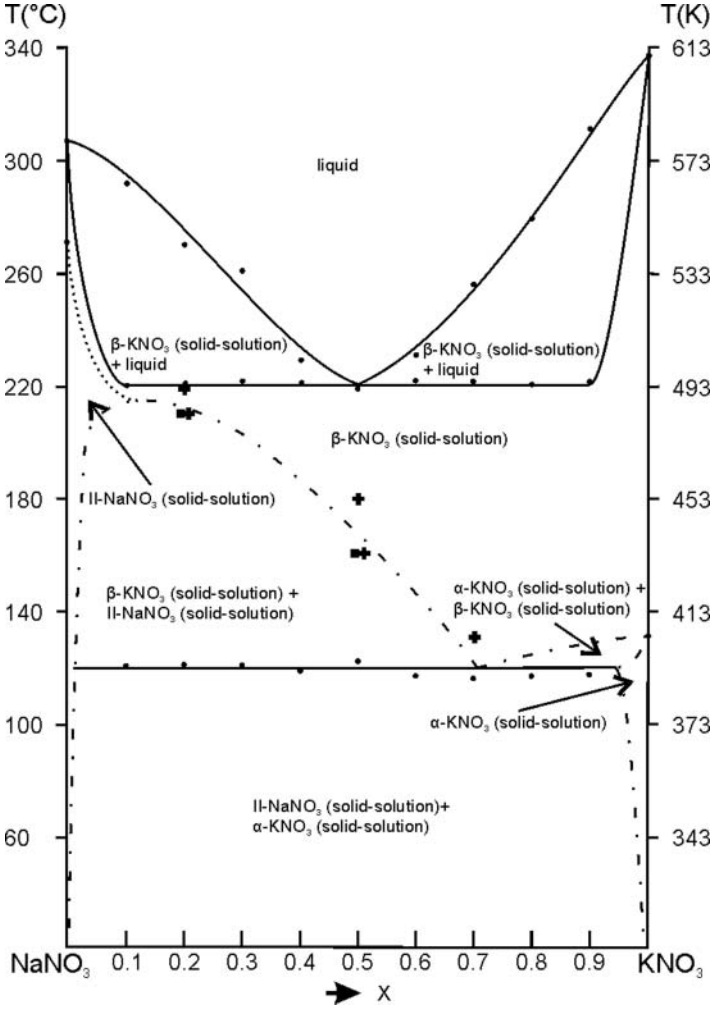

Figure 7. $NaNO_3-KNO_3$ phase diagram. Points: experimental DSC temperatures; plus sign: β-KNO_3 solid solution type; squares: II-$NaNO_3$ solid solution type. Experimental XRD points are only depicted in the vicinity of the solvus line.

Downloaded by [University Library Utrecht] at 06:48 27 January 2016

invariant, we observed a very asymmetric immiscibility gap and a large domain of β-KNO_3 solid solution type, which is present throughout compositions for certain temperature ranges. The second-order transition (or λ transition) can end wherever but we chose at the top of this immiscibility gap for the sake of simplicity. Finally, solid−liquid biphasic equilibrium with a flat minimum at 495 K was inferred.

Thermodynamic assessment

The aim of our thermodynamic analysis is two-fold. On the one hand, it aims to explore to which extent the underlying system complies with the general characteristics found for mixed crystals. On the other hand, it aims to assess to which extent the phase diagram, Figure 7, is consistent with the thermochemical data that are available for the system itself.

Downloaded by [University Library Utrecht] at 06:48 27 January 2016

To start with, and as regards the characteristics of mixed crystals, recent research has shown that their thermodynamic mixing properties are well accounted by the $AB\theta$ model for the excess Gibbs energy, see Oonk and references therein.[30]

In terms of the $AB\theta$ model, the molar excess Gibbs energy, as a function of temperature and mole fraction of the second component (here KNO_3) is given by the following expression:

$$G^E(T,X) = A\,X(1-X)\left(1-\frac{T}{\theta}\right)\,[1+B\,(1-2X)], \tag{1}$$

where A, B and θ are system-dependent parameters. The parameter A (in J·mol^{-1}) represents the magnitude of the excess function; θ (in K) the function's dependence on temperature; and B (dimensionless) the asymmetry of the function. The form in X between the square brackets has the advantage that the excess function of the equimolar mixture does not contain the parameter B.

The fact that G^E is linear in temperature implies that the excess enthalpy does not change with temperature:

$$H^E(T,X) \to H^E(X) = A\,X(1-X)\;[1+B(1-2X)]. \tag{2}$$

Another characteristic of the $AB\theta$ model is the fact that the mole fraction of the critical point of mixing (X_c) is the solution of the quadratic equation:

$$(18B)X^2 - (2+18B)X + (1+3B) = 0. \tag{3}$$

Next, the critical temperature of mixing (T_c) is obtained on the substitution of X_c's value in

$$T(X_c) = \frac{[2A + 6AB(1-2X_c)]X_c(1-X_c)}{R + (1/\theta)[2A + 6AB(1-2X_c)]X_c(1-X_c)}\;. \tag{4}$$

An intriguing aspect of mixed crystals is the existence of an empirical relationship between the value of the model parameter θ and the melting temperature (T_m) of the equimolar mixture:

$$\frac{\log(\theta/K)}{\log(T_m/K)} = 1.10 \pm 0.05. \tag{5}$$

At this place, we may observe that the melting point of the equimolar mixture together with the coordinates of the critical point of mixing are capable of giving a first impression of the values of the system-dependent parameters A, B and θ.

For the system at hand, we have $T_m = 494$ K; $T_c = 448$ K and X_c between 0.4 and 0.5. The last of these values goes well with $B = 0.1$, for which $X_c = 0.43$. An opening to the value of θ is offered by Equation (5): $\theta = 920$ K; for $T_m = 494$ K. The value of parameter A follows from Equation (4) with $T_c = 448$ K; $B = 0.1$; $\theta = 920$ K; $X_c = 0.43$; and the value of 8.314472 J·mol^{-1}·K^{-1} for the gas constant R; the result is $A = 14250$ J·mol^{-1}.

In the remaining part of our analysis, we concentrate on the change from solid to liquid of the equimolar mixture in terms of thermochemistry. The key thermochemical quantities are the change in enthalpy and the change in the Gibbs energy. The limited influence of the difference between the heat capacities of the liquid and solid states will be ignored.

The change in enthalpy is an opening to the difference between the excess enthalpies of liquid and solid. Likewise, the change in the Gibbs energy is an opening to the difference between the excess Gibbs energies of liquid and solid. The numerical values that are needed for our calculations are taken from Rogers and Janz.[36] Their data are essentially the same as ours, see Table 2, though somewhat more precise.

For the equimolar mixture, the change in enthalpy from solid to liquid is given by the expression

$$\Delta H(X=0.5) \;=\; 0.5\;\Delta H^*_A \;+\; 0.5\;\Delta H^*_B + \;\Delta H^{\mathrm{E}}\;(X=0.5), \tag{6}$$

in which $\Delta H^*{}_A$ and $\Delta H^*{}_B$ stand for the enthalpies of melting of pure $A = NaNO_3$ and pure $B = KNO_3$; an asterisk as a superscript is used to refer to a pure-component quantity. After substitution of the experimental data, Equation (6) changes into

$$9370 = 0.5\times 15440 + 0.5\times 10020 + \Delta H^E(X=0.5)/\mathrm{J{\cdot}mol^{-1}}. \tag{7}$$

From Equation (7), the equimolar change in excess enthalpy is calculated as

$$\Delta H^E(X=0.5) = -3360\ \mathrm{J{\cdot}mol^{-1}}. \tag{8}$$

Unlike the difference in enthalpy, the difference in the Gibbs energy is not independent of temperature:

$$\Delta G(T, X=0.5) = 0.5\Delta G^*_A(T) + 0.5\Delta G^*_B(T) \;+\Delta G^{\mathrm{E}}\;(T, X=0.5). \tag{9}$$

The quantities $\Delta G^*{}_A(T)$ and $\Delta H^*{}_B\,(T)$ which represent the change in the Gibbs energy on melting, are composed of an enthalpy and an entropy part as

$$\Delta G^*_A(T) = \Delta H^*_A - T\Delta S^*_A, \text{ and similar for component } B, \tag{10}$$

in which $\Delta S_A{}^*$, the entropy of melting, is the quotient of A's enthalpy of melting and its melting point.

Inserting all numerical values in Equations (9) and (10) for $T = 494$ K, one obtains

$$\Delta G(T=494K, X=0.5) = 0 = \\ 0.5(15440 - 26.67\times 494) + 0.5(10020 - 16.48\times 494) + \Delta G^E(T=494K,\ X=0.5). \tag{11}$$

In the first line of Equation (11), the zero between the two signs of equality is to indicate that the difference in the Gibbs energy is zero. This is the consequence of the fact that the two phases in equilibrium have the same composition, which is $X = 0.5$. From Equation (11),

$$\Delta G^E(X=0.5) = -2072\ \mathrm{J{\cdot}mol^{-1}}. \tag{12}$$

The last step of the evaluation of the equimolar excess properties of the mixed crystalline solid state is shown in Table 3.

In Table 3, the data for the liquid state are based on experimental heat of mixing data published by Kleppa.[70] These data were subjected to the empirical relationships found

Downloaded by [University Library Utrecht] at 06:48 27 January 2016

Table 3. Equimolar excess enthalpies and excess Gibbs energies at $T = 494$ K in J·mol^{-1}.

	Excess entalpy	Excess Gibbs energy
Liquid*	−525	−350
Liquid−solid	−3360	−2072
Solid	2835	1722

Note: *data derived by Ref. [70].

for binary liquid mixtures of common-ion alkali halides, to yield the excess values of −525 and −350 J·mol^{-1}.[71,72]

Through Equations (1) and (2), the solid state data in Table 3 give rise to $A = 11340$ J·mol^{-1} and $\theta = 1258$ K. Along with $B = 0.1$, the computed A and θ yield 448 K for the critical temperature of solid mixing, which is precisely the experimental temperature.

The fact that the computed result, $T_c = 448$ K, coincides with the experimental value for the critical temperature is satisfactory. A fact is, of course, that the outcome of the computations is sensitive to changes in the input data. The outcome is especially sensitive to the numerical value of the (difference) excess Gibbs energy. To give an example: when the excess Gibbs energy of the liquid is changed from −350 to −250 J.mol^{-1}, all other things being equal, the value of θ changes from 1258 to 1383 K, and subsequently the critical temperature from 448 to 463 K.

The outcome of the thermodynamic analysis is summarized in Table 4.

The numerical values in the bottom row of Table 4 for the three parameters model of the solid state, along with the melting properties of the pure components and the excess properties of the liquid state, were used to calculate the phase diagram. More precisely, the diagram the system would have if there were no phase transition in solid sodium nitrate. The calculated diagram is shown in Figure 8. The opening angle of the two-phase

Table 4. Survey of the outcome of the analysis; numbers between parentheses are input data.

	A (J·mol^{-1})	B	θ (K)	T_c (K)
Minimum 494 K + Equation (5)	14,250	(0.1)	920	(448)
Thermochemical data	11,340	(0.1)	1258	448

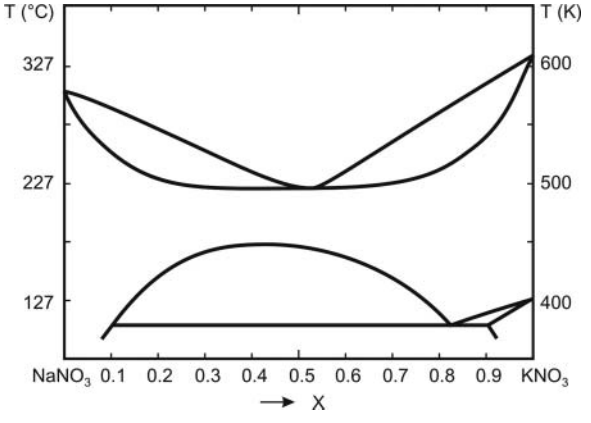

Figure 8. Calculated phase diagram using the $AB\theta$ model.

Downloaded by [University Library Utrecht] at 06:48 27 January 2016

region in the lower right-hand corner of the diagram was calculated using Van't Hoff's law (see Oonk and Calvet).[68]

An inspection of Figures 7 and 8 reveals that the two diagrams look very much alike. Clearly, the $AB\theta$ model is fully capable of giving a thermodynamically sound description of the sub-solidus solid state. In this respect, the $NaNO_3 + KNO_3$ system's behaviour is fully in line with the behaviour elucidated for the alkali halide systems, and mixed-crystal systems in general.

Our calculated and experimental results agree very well in the sense that the calculated diagram reproduces the asymmetric miscibility gap and the high-temperature single-phase domain.

Discussion

The $NaNO_3-KNO_3$ phase diagram has been studied for more than 150 years. As outlined in this paper, it is easy to understand the difficulties in developing an accurate unique phase diagram. While some studies demonstrated the presence of solid−liquid equilibrium with a minimum, others justify a eutectic invariant. It is, in fact, not surprising because the system is complex and certain experimental precautions must be considered. Transition kinetics, metastability and second-order transition are difficulties that arise from the experimental study. The diagram presented here is a representation of equilibrium state.

Figure 1 shows, as much as possible, the polymorphic behaviour of $NaNO_3$ and KNO_3. It is important to consider that a necessary but not sufficient condition to achieve total miscibility in solid state is that components crystallize in the same spatial group. At room temperature, phase II $NaNO_3$ crystallizes in the $R\bar{3}c$ spatial group and the α-KNO_3 phase crystallizes in the Pnma group. Total miscibility at room temperature is impossible. Our experimental and theoretical results show that the miscibility at the room temperature in this binary system is reduced. However, the situation is more complicated because if KNO_3 is melted, then the γ-KNO_3 phase is formed during the cooling and coexistence of II-$NaNO_3$ and γ-KNO_3 becomes possible. Nevertheless, in this case, total miscibility is also impossible (γ-KNO_3 crystallizes in the R3m group). In conclusion, an immiscibility gap is theoretically expected and experimentally confirmed at room temperature for this binary system.

At higher temperatures (401 K), Pnma α-KNO_3 transforms into an $R\bar{3}m$ β-KNO_3 by a first-order transition. Following the phase rule, a two phase domain with α-KNO_3 and β-KNO_3 is required. Effectively, our experimental and theoretical results show us this two solid phase domain. The first-order transition conduces to a eutectoid invariant at 393 K, and to a high-temperature miscibility domain, thus the solid−liquid equilibrium is present. Equilibrium between two solid solutions, one rich in II-$NaNO_3$ and the other rich in β-KNO_3, exists.

For sodium nitrate, a second-order transition from the II-$NaNO_3$ phase to the I-$NaNO_3$ phase is present. The $R\bar{3}m$ I-$NaNO_3$ phase is isostructural with the high temperature $R\bar{3}m$ β-KNO_3. Second-order transitions are not always considered in the literature for the phase diagram determination; however, in this case, it is crucial for the isomorphic relationships analysis between $NaNO_3$ and KNO_3. For this transition type, only the final temperature can be determined by a DSC analysis.

The question that has remained unanswered for over 150 years is: Does the solvus intersect with the solidus? To solve this question, experimental precautions regarding metastability must be taken into account. To achieve equilibrium at a high temperature, a minimum of 48 hours is required (depending on the composition and the temperature).

Downloaded by [University Library Utrecht] at 06:48 27 January 2016

Without this annealing period, a metastable mixture of different phases is observed. A solid solution (named in this study as β-KNO_3 solid solution) between isostructural R$\bar{3}$m I-$NaNO_3$ and R$\bar{3}$m β-KNO_3 exists. In some compositions, it is only present within a narrow temperature range just below the solidus line. At this stage, we can confirm that I-$NaNO_3$ and β-KNO_3 are isomorphous, that the binary system between $NaNO_3$ and KNO_3 is a system with high-temperature total miscibility, and that the solid−liquid equilibrium is a two-phase domain with a minimum.

At the atomic level, R$\bar{3}$m I-$NaNO_3$ and R$\bar{3}$m β-KNO_3 are essentially the same. Static and dynamic disorder has been proposed for β-KNO_3, see Nimmo and Lucas [20] and references therein for more information. They proposed that the NO_3^- group is not planar (in KNO_3) and thus a structural difference between I-$NaNO_3$ and β-KNO_3 is possible (although they have the same space group). In contrast, Stromme [31,73] made least squares refinement of both R$\bar{3}$m structures, I-$NaNO_3$ (at 563 K) and β-KNO_3 (at 425 K) and arrived at the same solution: disorder at high temperature can be modelled in the same manner. Slight differences in the structures are accepted and thus, interchanging between Na^+ and K^+ is possible particularly at high temperatures. Therefore, we can say that R$\bar{3}$m I-$NaNO_3$ and R$\bar{3}$m β-KNO_3 are isomorphous at high temperature.

Conclusions

The main result of this work is the experimental phase diagram proposed. It has a eutectoid invariant at 393 K, with an extended immiscibility zone below this invariant, with very limited solid solutions at both extremes. Above the eutectoid invariant, there is an asymmetric immiscibility gap, and the $NaNO_3$ second order transition can end in the uppermost point of the immiscibility gap. A narrow $NaNO_3$ R$\bar{3}$c solid solution domain must exist below; however, this was not observed directly. Furthermore, at high temperatures, a β-KNO_3 solid solution is observed for all compositions, thus, the phase diagram shows a solid−liquid equilibrium with minimum. Therefore, I-$NaNO_3$ and β-KNO_3 are only isomorphous at high temperatures because they are isostructural, chemically analogous and can form a solid solution in all compositions.

Our study has revealed that slow transition kinetics for the formation of high-temperature solid solutions can explain the conflicting arguments that exist in the literature to solve whether the diagram is eutectic or melting point minimum.

Thermodynamic results of the analysis are not in conflict with the experimental evidence for (complete) subsolidus miscibility. Finally, the phase diagram of the system $NaNO_3$−KNO_3 and its thermodynamic mixing properties are fully in line with the general characteristics found for the mixed crystal systems.

Disclosure statement

No potential conflict of interest was reported by the authors.

Funding

This work was supported by the Ministerio de Ciencia y Tecnología [grant CICYT (MAT2011-27225)]; the Generalitat de Catalunya under grant Grup Consolidat [2009SGR1307], and Xarxa de Referència R+D+I en Materials Avançats per l'Energia (XaRMAE). And The Ministerio de Educación under grant la Factoría Cristalográfica [Consolider-Ingenio CSD2006-15]. R. Benages-Vilau acknowledges Abengoa enterprise for the financial support through a Cenit program Consorcio Solar de I+D ConSOLi+da.

Downloaded by [University Library Utrecht] at 06:48 27 January 2016

Downloaded by [University Library Utrecht] at 06:48 27 January 2016

References

[1] Berg RW, Kerridge DH. The $NaNO_3$-KNO_3 system: the position of the solidus and sub-solidus. Dalton Trans. 2004;15:2224−2229.

[2] Voskresenskaya NK, Evseeva NN, Berul SI. Handbook of solid-liquid equilibria in systems of anhydrous inorganic salts. Jerusalem: Keter Press; 1970. Part I, Binary systems with common anion; p. 7−602.

[3] Berg RW, Kerridge DH. Raman mapping in the elucidation of solid salt eutectic and near eutectic structures. J Raman Spec. 2002;33:165−172.

[4] Benes O, Konings R, Wurzer S, et al. A DSC study of the $NaNO_3$-KNO_3 system using an innovative encapsulation technique. Thermochim Acta. 2010;509:62−66.

[5] Ping W, Harrowell PBN, Angell CA. Composition dependence of the solid state transitions in $NaNO_3$/KNO_3 mixtures. Thermochim Acta. 2009;486:27−31.

[6] Rao CNR, Prakash B, Natarajan M. Crystal structure transformations in inorganic nitrites, nitrates, and carbonates. National Standard Reference Data System − National Bureau of Standards; 1975.

[7] Benages-Vilau R, Calvet T, Cuevas-Diarte MA. Polymorphism, crystal growth, crystal morphology and solid state miscibility of alkali nitrates. Crystall Rev. 2014;20(1):25−55.

[8] Paul GL, Pryor AW. Study of sodium-nitrate by neutron diffraction. Acta Cryst B. 1972;28:2700−2702.

[9] Gonschorek G, Weitzel H, Miehe G, et al. The crystal structure of $NaNO_3$ at 100 K, 120 K, and 563K. Zeitschrift für Kristallographie. 2000;215:752−756.

[10] Fermor JH, Kjekshus A. On the electrical properties of $NaNO_3$. Acta Chem Scand. 1968;22:1628−1636.

[11] Parsonage NG, Staveley LAK. Disorder in crystals. Oxford: Clarendon Press; 1978.

[12] Klement WJ. Variation of λ transition temperature in $NaNO_3$-base binary alloys with $AgNO_3$, KNO_3, and NaNO2. J Inorg Nucl Chem. 1974;36:1916−1918.

[13] Antao SM, Hassan I, Mulder WH, et al. The R-3c → R-3 m transition in nitratine, $NaNO_3$, and implications for calcite, $CaCO_3$. Phys Chem Minerals. 2008;35:545−557.

[14] Antao SM, Hassan I, Mulder WH, et al. In situ of the R-3c →R-3 m orientational disorder in calcite. Phys Chem Minerals. 2009;36:159−169.

[15] Ballirano P. Laboratory parallel-beam transmission X-ray powder diffraction investigation of the thermal behavior of nitratine $NaNO_3$: spontaneous strain and structure evolution. Phys Chem Minerals. 2011;38:531−541.

[16] Harris MJ. A new explanation for the unusual critical behaviour of calcite and sodium nitrate, $NaNO_3$. Am Mineralogist. 1999;84:1632−1640.

[17] Zamali H, Jemal M. Diagrammes de phases des systemes binaires KNO_3-$CsNO_3$ et KNO_3-$NaNO_3$. J Thermal Anal. 1994;41:1091−1099.

[18] Dessureault Y, Sangster J, Pelton AD. Evaluation critique des donées thermodynamiques et des diagrammes de phases des systèmes AOH-AX, ANO_3-AX, ANO_3-BNO_3, AOX, BOX où A, B = Li, Na, K Et X = Cl, F, NO_3, OH. J Chim Phys. 1990;87:407−453.

[19] Chen A, Chernow F. Nature of ferroelectricity in KNO_3. Phys Rev. 1967;154:493−505.

[20] Nimmo JK, Lucas BW. The crystal structures of γ- and β-KNO_3 and the α, β,γ phase transformations. Acta Cryst. 1976;B-32:1968−1971.

[21] Shimada S, Aoki T. Stabilization of the ferroelectric γ-phase by doping with Na^+ determined by the acoustic emision method. Chem Lett. 1996;393−394

[22] Christensen AN, Norby P, Hanson JC, et al. Phase transition of KNO_3 monitored by sincrotón X-ray powder diffraction. Appl Cryst. 1996;29:265−269.

[23] Westphal MJ. Particle size and cooperative behaviour effects on KNO_3 phase transitions. J Appl Phys. 1993;74:6107−6114.

[24] Westphal MJ. Cooperative behavior during ferroelectric transition in KNO_3 powder. J Appl Phys. 1993;74:3131−3136.

[25] Westphal MJ, Wood JW, Redin RD, et al. Calorimetric and photoacustic investigation of KNO_3 phase transition. J Appl Phys. 1993;73:7302−7310.

[26] Shimada S, Katsuda Y, Inagaki M. Phase transition of potassium nitrate monitored by acoustic emission technique and the healing effect on the γ-α transition. J Phys Chem. 1993;97:8803−8807.

[27] Poprawski R, Rysiakiewicz-Pasek E, Sieradzki A, et al. Ferroelectric phase transitions in KNO_3 embedded into porous glasses. J Non Cryst Solids. 2007;353:4457−4461.

[28] Baryshnikov SV, Charnaya EV, Milinkiy AY, et al. Phase transition in $K_{1-x}Na_xNO_3$ embedded into molecular sieves. J Phys Cond Mat. 2009;21:325902.
[29] Fermor JH, Kjekshus A. On the electrical properties of KNO_3. Acta Chemica Scandinavica. 1967;21:1265–1276.
[30] Oonk HAJ. Solid-state solubility and its limits. The alkali halide case. Pure Appl Chem. 2001;73:807–823.
[31] Stromme KO. On the crystal structure of potassium nitrate in the high temperature phases I and III. Acta Chemica Scandinavica. 1969;23:1625–1636.
[32] Xu K, Chen Y. Raman spectroscopic studies of mixed crystals of $NaNO_3$-KNO_3 quenched from different temperatures: evidence for limited solid solutions in the system. J Raman Spectrosc. 1999;30:441–448.
[33] Greis O, Bahamadan KM, Uwais BM. The phase diagram of the system $NaNO_3$-KNO_3 studied by differential scanning calorimetry. Thermochim Acta. 1985;86:343–350.
[34] Kramer CM, Wilson CJ. The phase diagram of $NaNO_3$-KNO_3. Thermochim Acta. 1980;42:253–264.
[35] Kamimoto M. Thermodynamic properties of 50 Mole% $NaNO_3$-$50KNO_3$ [HTS_2]. Thermochim Acta. 1981;49:319–331.
[36] Rogers DJ, Janz GJ. Melting-crystallization and premelting properties $NaNO_3$-$NaNO_3$ enthalpies and heat capacities. J Chem Eng Data 1982;27:424–428.
[37] Abe O, Utsunomiya T, Hoshino Y. The thermal stability of binary alkali metal nitrates. Thermochim Acta. 1984;78:251–260.
[38] Zamali H, Jriri R, Rogez J, et al. Mixing properties in the continuous solid solution of the system KNO_3-$NaNO_3$. Thermochim Acta. 1994;233:111.
[39] Zhang X, Tian J, Xu K, et al. Thermodynamic evaluation of phase equilibria in $NaNO_3$-KNO_3 systems. J Phase Equilibria. 2003;24:441–446.
[40] Tammann VG, Ruppelt A. Die entmischung lückenlose mischkristallreihen [The segregation gaps of solid solution series]. Zeitschrift für anorganische und allgemeine Chemie. 1931;197:65–89.
[41] Hissink DJ. On the formation and conversion of mixed crystals from sodium nitrate and potassium nitrate and from sodium nitrate with silver nitrate. Z Phys Chem. 1900;32:537–563.
[42] Madgin WM, Briscoe HVA. The melting point [solidus] curve for mixtures of potassium nitrate and sodium nitrate. J Chem Soc. 1923;123:2914–2916.
[43] Briscoe HVA, Madgin W M. The freezing point curve for mixtures of potassium nitrate and sodium nitrate. J Chem Soc. 1923;123:1608–1618.
[44] Kofler VA. Über Periodische Umlagerungen Beim Kristallisieren Und Schmelzen Von Mischkristallen Z Elektrochem. [Rearrangements crystallization and melting of mixed crystals]. 1955;59:939–941.
[45] Bartlett HE, Johnson KE. Electrolytic reduction and ellingham diagrams for oxy-anions systems. Can J Chem. 1966;44:2119–2129.
[46] Freeman ES. The kinetics of the thermal decomposition of sodium nitrate and of the reaction between sodium nitrite and oxygen. J Phys Chem. 1956;60:1487–1493.
[47] Freeman ES. The kinetics of the thermal decomposition of potassium nitrate and of the reaction between potassium nitrite and oxygen. J Am Chem Soc. 1957;79:838–842.
[48] Alexander JJ, Hindin SG. Phase relations in heat transfer salt systems. Ind Eng Chem. 1947;39:1044–1049.
[49] Bartholomew RF. A study of the equilibrium $KNO_3[l] \leftrightarrow KNO_2[l] + 1/2O_2[g]$ over the temperature range 550–750 °C. J Phys Chem. 1966;70:3442–3446.
[50] Carling RW. Heat capacities of $NaNO_3$ and KNO_3 from 350 to 800 K. Thermochim Acta 1983;60:265–275.
[51] Iwadate Y, Okada I, Kawamura K. Density and heat capacity of molten $NaNO_2$-KNO_3 mixtures. J Chem Eng Data. 1982;27:288–290.
[52] Robelin C, Chartrand P, Pelton AD. Thermodynamic evaluation and optimization of the ($NaNO_3 + KNO_3 + Na_2SO_4 + K_2SO_4$) System. J Chem Thermodyn. 2015;83:12–26.
[53] Xu K, Chen Y. Temperature-dependent raman spectra of mixed crystals of $NaNO_3$-KNO_3: evidence for limited solid solution. J Raman Spectrosc. 1999;30:173–179.
[54] Laybourn K, Madgin WM. On the measurement of mechanical properties of binary inorganic salt mixtures. J Chem Soc. 1932;28:857–866.

Downloaded by [University Library Utrecht] at 06:48 27 January 2016

[55] Eweka EI, Kerridge DH. Non-ideal change of electrical conductivity on solidification and remelting of salt eutectics: 1. Oxyanion-based systems. Solid State Ionics. 2006;177: 1245–1250.
[56] Eweka IE, Kerridge DH. Changes in electrical conductivity of salt eutectic through the melting point. Phys Let A. 1993;174:441–442.
[57] Moreno E, Cordobilla R, Calvet T, et al. Polymorphism of even saturated carboxilic acid from n-decanoic to n-eicosanoic acid. New J Chem. 2007;31:947–957.
[58] Gbbode G, Negrier P, Mondieig D, et al. Polymorphism and solid-state miscibility in the pentadecanoic acid-heptadecanoic acid binary system. Chem Phys Lipids 2008;154:68–77.
[59] Metivaud V, Lefevre A, Ventolà L, et al. Hexadecane [$C_{16}H_{34}$] 1-hexadecanol [$C_{16}H_{33}OH$] binary system: crystal structures of the components and experimental phase diagram. Application to thermal protection of liquids. Chem Mat. 2005;17:3302–3310.
[60] Ventolà L, Calvet T, Cuevas-Diarte MA, et al. Solid-solid and solid-liquid equilibria in the n-alkanols family: $C_{18}H_{37}OH$-$C_{20}H_{41}OH$ system. Phys Chem Chem Phys. 2004;6:3726–3731.
[61] Ventolà L, Metivaud V, Bayés L, et al. The binary system tetradecanedioic acid-hexadecanedioic acid: polymorphism of the components and experimental phase diagram. Helvetica Chim Acta. 2006;89:2027–2039.
[62] Ventolà L, Bayés L, Benages R, et al. Decanedioic acid [$C_{10}H_{18}O_4$]/dodecanedioic acid [$C_{12}H_{22}O_4$] system: polymorphism of the components and experimental phase diagram. Helvetica Chim Acta. 2008;91:1286–1298.
[63] Quality chemicals [Internet]. Spain. Available from: http://www.qualitychemicals.com/cas/index.html
[64] Courchinoux R, Chanh NB, Haget Y, et al. Du Signal aux Phénomènes: Une Approche Pratique l'Établissement des Diagrammes de Phases par Analyse Thermique [Signal to phenomena: a practical approach to establishment of the phase diagrams of by thermal analysis]. J Chim Phys. 1989;86:561–593.
[65] Materials studio modeling 4.2. [Internet]. Available from: http://accelrys.com/products/materials-studio
[66] Neumann M. X-Cell: a novel indexing algorithm for routine tasks and difficult cases. J Appl Cryst. 2003;36:356–365.
[66] Pawley GS. Unit-cell refinement from powder diffraction scans. J Appl Cryst. 1981;14:357–361.
[68] Oonk HAJ, Calvet T. Equilibrium between phases of matter: phenomenology and thermodynamics. Dordrecht: Springer; 2008.
[69] Nakamoto K. Inorganic compounds; infrared and raman spectra of inorganic and coordination compounds. New York (NY): Wiley; 1986.
[70] Kleppa OJ. A new twin high-temperature reaction calorimeter. The heats of mixing in liquid sodium-potasium nitrates. J Phys Chem. 1960;64:1937–1940.
[71] Oonk HAJ, Bouwstra JA, van Ekeren PJ. Binary common-anion alkali halides mixtures, correlation of the thermochemical and phase diagram data. Calphad. 1986;10:137–161.
[72] van der Kemp WJM, Blok JG, van Genderen ACG, et al. Binary common-ion alkali halide mixtures: a uniform description of the liquid and solid state. Thermochim Acta. 1992;196:301–315.
[73] Stromme KO. The crystal structure of sodium nitrate in the high temperature phase. Acta Chemica Scandinavica. 1969;23:1616–1624.

Downloaded by [University Library Utrecht] at 06:48 27 January 2016